Kinetics of Dissociation of Reduced Nicotinamide Adenine Dinucleotide Phosphate from Its Complexes with Malic Enzyme in Relation to Substrate Inhibition and Half-of-the-Sites Reactivity†

K. Dalziel,‡ R. Y. Hsu,*,§ B. Matthews, and J. M. Soulié

ABSTRACT: Malic enzyme of pigeon liver binds NADPH at four equivalent enzyme sites and binds Mn^{2+} and malate each at two sets of "tight" and "weak" sites with negative cooperativity [Pry, T. A., & Hsu, R. Y. (1980) *Biochemistry 19*, 951–962]. Stopped-flow studies on the displacement of NADPH from the malate–enzyme complexes E_4–$NADPH_4$, E_4–Mn_2^{2+}–$NADPH_4$, E_4–Mn_2^{2+}–$NADPH_4$–dimalate, and E_4–Mn_2^{2+}–$NADPH_4$–tetramalate by large excess $NADP^+$ or its analogue phosphoadenosine(2′)diphospho(5′)ribose show that NADPH dissociates from the binary complex rapidly with a first-order rate constant of 427 s^{-1}. Dissociation from the ternary E_4–Mn_2^{2+}–$NADPH_4$ complex containing two tightly bound Mn^{2+} ions can be described by a single first-order process with a rate constant of 135 s^{-1}, or more satisfactorily by two simultaneous first-order processes attributable to the reactions of Mn^{2+}-deficient ($k \simeq 427$ s^{-1}) and Mn^{2+}-liganded ($k = 96$ s^{-1}) subunits. The latter equals twice the maximum steady-state turnover rate of 53.2 + 3.0 s^{-1} assigned to dissociation of the reduced nucleotide from transient E–Mn^{2+}–NADPH, and this 2:1 ratio strongly supports our proposed "half-of-the-sites" model [Hsu, R. Y., & Pry, T. A. (1980) *Biochemistry 19*, 962–968]. Dissociation from the E_4–Mn_2^{2+}–$NADPH_4$–dimalate complex ($k = 100$ s^{-1}) follows only the slower process, suggesting that occupancy of malate at two sites tightens enzyme-bound NADPH on the adjacent sites. Binding of malate at two additional weak sites yields E_4–Mn_2^{2+}–$NADPH_4$–tetramalate and a NADPH dissociation rate constant of 2.69 s^{-1}. The 97% decrease in NADPH dissociation parallels the observed 93% maximal inhibition by malate and is the cause of substrate inhibition. The slow onset of substrate inhibition is a first-order process consistent with a slow malate-induced conformational change of the quaternary complex from an active to a less active form.

Malic enzyme from pigeon liver catalyzes the oxidative decarboxylation of malate via a preferentially ordered kinetic mechanism in which $NADP^+$ or the activator (Mn^{2+} or Mg^{2+}) binds first, followed by malate, with the release of CO_2, pyruvate, and NADPH (Hsu et al., 1967). Dissociation of NADPH, the final product, has been implicated as the rate-limiting step of this reaction (Schimerlik et al., 1977; Reynolds et al., 1978; Pry & Hsu, 1980). While this enzyme obeys Michaelian kinetic behavior at low substrate and activator concentrations, it is strongly inhibited by high malate concentrations (>0.3 mM), and this inhibition is quantitatively relieved by increasing concentrations of activating metal ions (Hsu et al., 1976; Reynolds et al., 1978; Hsu & Pry, 1980; Hsu, 1983). Heterogeneous binding of Mn^{2+} and malate, but not $NADP^+$, is also detectable in equilibrium binding experiments which indicate the presence of two types of sites for each reactant on the enzyme tetramer, with affinities differing by more than an order of magnitude.

A novel "half-of-the-sites" model has been postulated in a recent study to account for the unusual behavior of the enzyme (Hsu & Pry, 1980). During catalysis, only two "tight" sites are simultaneously undergoing turnover, and the remaining sites regulate this rate under conditions of excess malate by substrate inhibition. This model is also consistent with other reported properties of the enzyme such as a maximum burst of enzyme-bound NADPH equal to half of the enzyme sites, half-of-the-sites binding of the transition-state analogue oxalate, and half-of-the-sites reactivity of bromopyruvate in affinity labeling experiments (Reynolds et al., 1978; Pry & Hsu, 1980; Hsu & Pry, 1980; Chang & Hsu, 1973, 1977; Vernon & Hsu, 1983).

Corollary to the postulated model and with NADPH release rate limiting, this final step is expected to double the rate of turnover in order to account for the presence of "noncatalytic" subunits. This 2:1 ratio is now confirmed by direct determination of the NADPH dissociation rate constant from malic enzyme–NADPH complexes by using the stopped-flow technique. At high malate concentration, the rate constant decreases 37-fold, demonstrating that malate-induced inhibition of the NADPH dissociation step is responsible for substrate inhibition.

Materials and Methods

Triethanolamine hydrochloride, tris(hydroxymethyl)-aminomethane hydrochloride (Tris-HCl), $NADP^+$ (K salt, 99% pure), and NADPH are from Boehringer. L-Malic acid, dithiothreitol, and phosphoadenosine(2′)diphospho(5′)ribose (ATPR) are from Sigma. Reagent-grade manganous chloride is obtained from Fison's. Pigeon liver malic enzyme is prepared by an affinity chromatographic procedure (A. Reddy, J. M. Soulié, and R. Y. Hsu, unpublished results) with approximately 50% yield and a maximum specific activity of 60 μmol of $NADP^+$ consumed min^{-1} (mg of enzyme)$^{-1}$ at 30 °C. The purified enzyme is homogeneous in polyacrylamide gel electrophoresis (PAGE) and sodium dodecyl sulfate–polyacrylamide gel electrophoresis (SDS–PAGE) gels. It has a tetramer molecular weight of 260 000 and subunit molecular weight of 65 000 (Nevaldine et al., 1974). The purified enzyme containing bound $NADP^+$ (used as the eluent in affinity chro-

† From the Department of Biochemistry, University of Oxford, Oxford OX1 3QU, England, and the Department of Biochemistry, State University of New York, Upstate Medical Center, Syracuse, New York 13210. *Received April 13, 1983.* Supported by the British Science Research Council and a grant (AM 13390) from the National Institutes of Health.

‡ Member of the Oxford Enzyme Group.

§ Guest Research Fellow of the Royal Society. Permanent address: Department of Biochemistry, State University of New York, Upstate Medical Center, Syracuse, NY 13210.

0006-2960/83/0422-5359$01.50/0 © 1983 American Chemical Society

matography) in 30 mM Tris-HCl buffer, pH 7.5, 1 mM each of dithiothreitol and EDTA, and 10% glycerol is stable at −70 °C for several months.

Prior to each experiment, the enzyme is thawed and dialyzed overnight against 50 mM triethanolamine hydrochloride buffer, pH 7.0. To each 1 mL of enzyme solution containing approximately 10 mg of protein is added 200 mg of charcoal suspension; the mixture is then stirred 10 min and centrifuged twice to affect removal of particles. The resulting enzyme solution is completely active and is free of bound nucleotide as indicated by an A_{280}/A_{260} ratio of 1.9–2.0. The charcoal suspension is prepared from commerical grade activated charcoal by pulverization, followed by thorough washing in H_2O, 6 N HCl, H_2O, and 50 mM triethanolamine hydrochloride buffer, pH 7.0, and centrifugation to remove excess liquid. The suspension is stored at 4 °C before use.

Malic enzyme activity is assayed according to Hsu & Lardy (1967a,b). Protein concentration is determined at 278 nm by using an extinction coefficient of 0.86 for a 0.1% (w/v) nucleotide-depleted protein solution.

Fluorescence Stopped-Flow Apparatus. The apparatus is basically as described by Gibson & Milnes (1964), except the hydraulic drive is replaced by a pneumatic drive (Durrum Instruments) and the 20-mm path-length observation tube is replaced by a fluorescence cell, which is a quartz tube with a 6 cm × 3 mm internal diameter, mounted in the observation tube block and cemented to the mixing chamber. A horizontal hole in the block admits the exciting light, and the fluorescence emission is transmitted through a slit (5 mm × 2 mm) and a vertical hole in the block to a photomultiplier. A quartz rod used as a light guide increases the sensitivity 8-fold. A small cell containing 1 M $NaNO_2$ is used as a light filter to absorb scattered UV light. The fluorescence blank of the cell when filled with water is equivalent to that of 0.8 μM NADPH. The dead time and mixing efficiency measured as described by Dalziel et al. (1978) are 2 ms and 98%, respectively. The time constant of the apparatus can be varied from 0.15 to 10 ms. The light source is a 150-W xenon lamp with a monochromator (Bausch & Lomb, 33-86-50) and light filter (Corning CS7-54). The wavelength of the exciting light is 340 nm, and the monochromator slits correspond to nominal bandwidths of 6.6 and 9.9 nm.

The photomultiplier output is linked through a programmable real-time clock, triggered by the stopping syringe, and an analogue-to-digital converter (12 bit, full-scale deflection +5.12 V) to a PDP 11/03 computer with dual floppy discs (Digital Equipment Co.). The experiments are run by a computer program written in FORTRAN IV, with sampling rates up to 6000/s. For some experiments, the analogue-to-digital converter is sampled by a subroutine written in MACRO, which allows sampling rates up to 25 000/s. Digital voltage values are stored on disc for later analysis. They are also displayed through a digital-to-analogue converter on an oscilloscope screen for immediate visual check and can be printed out at the terminal.

Technique for Kinetic Studies. When NADPH binds to malic enzyme, its fluorescence with an excitation maximum at 340 nm is enhanced. This enhancement is further augmented by malate in the presence of $MnCl_2$. The kinetics of NADPH dissociation from binary, ternary, and quaternary enzyme–NADPH complexes are studied by recording the time course of fluorescence decay following the mixing of equal volumes of enzyme or complex with a high concentration of the displacement reagent, $NADP^+$ or ATPR. When present, $MnCl_2$ and malate are included in both syringes of the stopped-flow apparatus. All experiments are performed in 50 mM triethanolamine hydrochloride buffer, pH 7.0 at 30 °C. Fluorescence values of the appropriate blanks, such as buffer alone, buffer plus NADPH (and $MnCl_2$ and malate, if present), buffer plus NADPH plus enzyme, and buffer plus $NADP^+$ (or ATPR), are recorded for the purpose of calculations.

Digital voltages corresponding to the fluorescence (F_t) at 1000 equally spaced time intervals (Δt) are recorded during each kinetic experiment. Twenty more values are also recorded at longer intervals to allow estimation of the fluorescence at equilibrium. The data are analyzed subsequently with the computer by nonlinear regression fitting to the function for two exponentials

$$F_t = F_0(A_1e^{-k_1t} + A_2e^{-k_2t} + A_3) \quad (1)$$

using a FORTRAN program in which the appropriate subroutines from the Digital library are incorporated. In reactions where a fast component is present ($k = 427\ s^{-1}$), only early data are used for computation of its rate. Fitting to a single exponential is performed by setting $k_2 = 0$.

Initial Rate Measurements. The maximum turnover number for the enzyme in the oxidative decarboxylation of malate is determined by steady-state initial rate measurements in a sensitive fluorometer. This is a modification of the recording fluorometer described by Dalziel (1961, 1962) and Engle & Dalziel (1968). The mercury lamp in the original apparatus is replaced by a 100-W tungsten iodide lamp and stabilized power supply (Applied Photophysics Ltd). The Vibron electrometer and pen recorder are replaced by the A/D converter and PDP 11/03 computer used with the stopped-flow apparatus. The experiments are run with a computer program written in FORTRAN IV. During each initial rate measurement, the increasing voltage in the anode load of the photomultiplier caused by the NADPH fluorescence is sampled every 3 ms by the A/D converter for 1 min (or longer if required). The mean values during successive 1-s intervals are computed, stored on disc, and displayed as a progress curve on an oscilloscope screen through a D/A converter. The rate in micromolar per minute (±SD) is computed for the first and second halves of the reaction and printed out at the terminal, using the voltage given by the Perspex standard, which is recorded before each initial rate measurement. The NADPH equivalent of the Perspex standard (Dalziel, 1962) is put into the program at the beginning of the experiment. All the reagents are freed from dust and debris as described by Engle & Dalziel (1968). A signal of 5 V could easily be obtained from 1 μM NADPH. The sensitivity could be varied widely by the appropriate choice of anode load or dynode voltage.

Initial rates are also measured with a relatively large enzyme subunit concentration of 0.57 μM using the stopped-flow apparatus in the optical density mode. Enzyme, $MnCl_2$, and $NADP^+$ are placed in one syringe and malate and $MnCl_2$ in the other. After the components of the two syringes are mixed, the increase of optical density at 340 nm is recorded by the collection of 1000 digital voltage values in 1 s and appropriate calculation in the computer, using a program written in FORTRAN IV.

Results

Kinetics of NADPH Dissociation from the E–NADPH Complex. Figure 1A shows the time course of fluorescence decay accompanying release of free NADPH from the binary complex and displacement by large excess $NADP^+$. Divalent metal ions, Mg^{2+} or Mn^{2+}, which are essential for activity, are not present. From the dissociation constants (Pry & Hsu,

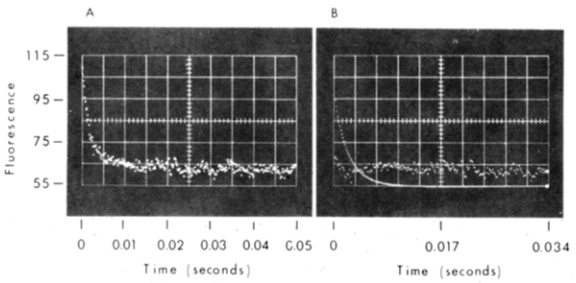

FIGURE 1: Fluorescence decay curves of NADPH dissociation from the E_4–$NADPH_4$ complex. The final concentrations are the following: enzyme subunits, 10.0 μM; NADPH, 9.5 μM, in triethanolamine hydrochloride buffer, pH 7.0 at 30 °C; 1.0 mM $NADP^+$ is used as the displacement reagent. (A) Time course; (B) simulated progress curve and residuals obtained by nonlinear regression fitting to a single exponential function. The rate constant is 410 s^{-1}. The residuals in this and other experiments are the differences between computed and experimental values, displaced upward in the figure to show both negative and positive values.

Table I: First-Order Rate Constants of NADPH Dissociation from the E-NADPH Complex[a]

[enzyme] (μM)	[NADPH] (μM)	displacer	displacer concn (mM)	k (s^{-1})
8.75	8.35	$NADP^+$	0.5	436 ± 26
10.0	9.5	$NADP^+$	1.0	418 ± 23
10.0	9.5	$NADP^+$	4.0	431 ± 72
10.0	9.5	$NADP^+$	10.0	463 ± 82
10.0	9.73	ATPR	1.0	385 ± 12

[a] The rate constants are the means (±SD) of values estimated by nonlinear regression fitting of four to eight progress curves in each experiment to a single exponential function.

1980) for coenzyme complexes and the concentrations employed (10.0 μM enzyme subunits, 9.5 μM NADPH, and 1.0 mM $NADP^+$), it is calculated that 75% of the total NADPH would be initially bound and 90% of this bound nucleotide would be displaced by $NADP^+$. The above progress curve is consistent with a simple first-order dissociation reaction, as shown by the exponential curve and residuals obtained by nonlinear regression fitting to eq 1 with $k_2 = 0$ (Figure 1B). From four such progress curves, a mean rate constant of 418 ● 23 s^{-1} is obtained. Other experiments are carried out with similar enzyme and NADPH concentrations using $NADP^+$ or ATPR as the displacement reagent. The results are summarized in Table I. The rate constants are identical within experimental error with a mean of 427 s^{-1} from five separate experiments. The displacement reaction (Fatania et al., 1982) may be written as

$$\begin{aligned} \text{E·NADPH} &\underset{k_2}{\overset{k_1}{\rightleftharpoons}} \text{NADPH} + \text{E} \\ \text{E} + \text{NADP}^+ \text{ (ATPR)} &\underset{k_4}{\overset{k_3}{\rightleftharpoons}} \text{E·NADP}^+ \text{ (ATPR)} \end{aligned} \qquad (2)$$

Although there is no analytical solution to the nonlinear differential equations which describe this reaction, the constancy of the observed rate constant over a wide range (20-fold) of $NADP^+$ concentrations or with ATPR, together with results of computer simulations of the time course with various assumed values for the rate constants k_1–k_4 carried out in similar studies on isocitrate dehydrogenase (Fatania et al., 1982), gives confidence that the observed rate constant in the present experiments is identical with k_1 in eq 2.

In the following experiments, NADPH to enzyme ratios of 0.95–2.0 are obtained by varying the NADPH concentration. The higher ratio increases NADPH site occupancy, while the useful amplitude for measurements is decreased due to a high background fluorescence of free NADPH. The experimental kinetic parameters are not detectably altered by a change in this ratio.

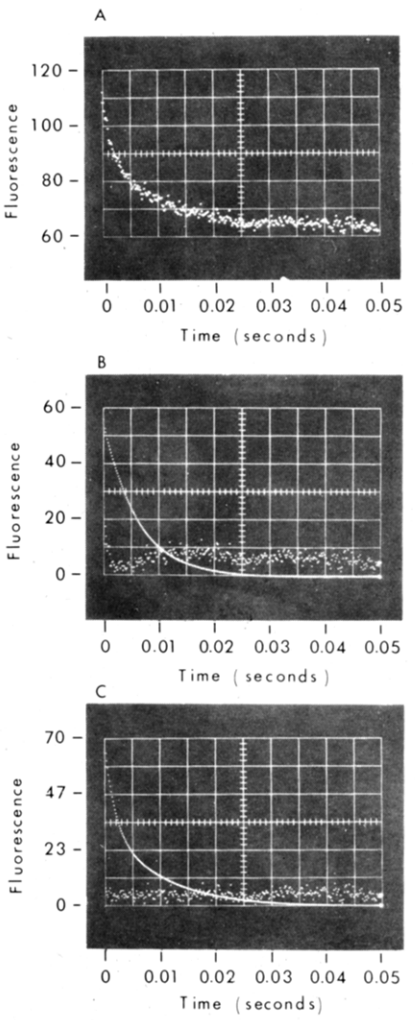

FIGURE 2: Fluorescence decay curves of NADPH dissociation from the enzyme complex in the presence of Mn^{2+}. The final concentrations are the following: enzyme subunits, 10.0 μM; $MnCl_2$, 0.2 mM; NADPH, 11.0 μM; 1.0 mM $NADP^+$ is used as the displacement reagent. (A) Time course; (B) simulated progress curve and residuals obtained by nonlinear regression fitting to a single exponential function, giving $k = 130$ s^{-1}; (C) simulated progress curve and residuals obtained by fitting to the sum of two exponentials, giving $k_1 = 651$ s^{-1} and $k_2 = 96$ s^{-1}.

Effect of Mn^{2+} on the Kinetics of NADPH Dissociation. Previously, we have reported that Mn^{2+} binds malic enzyme biphasically at two tight (k_t = 8 μM) and 2–4 weak ($k_w \simeq$ 0.9 mM) metal sites (Hsu et al., 1976). In these experiments, the kinetics of NADPH dissociation are monitored in the presence of 0.2 mM Mn^{2+}, sufficient to saturate both tight sites. A typical progress curve using 1.0 mM $NADP^+$ as the displacer is shown in Figure 2A. Nonlinear regression fitting of this curve to a single exponential function (Figure 2B) yields a rate constant of 130 s^{-1}, clearly lower than the value of 427 s^{-1} seen for the binary complex. Estimates of first-order rate constants using 1.0 mM $NADP^+$, or 0.83, 1.0, or 3.2 mM ATPR, are not significantly different, affirming the validity of determining the NADPH dissociation rate constant by the displacement reaction (eq 2). A mean value of 135 s^{-1} is obtained from five experiments. Close inspection of the residuals in Figure 2B indicates, however, that the fitting is poor in the first $\simeq$10 ms due to the presence, in addition, of a faster

Table II: First-Order Rate Constants and Amplitudes of NADPH Dissociation from the E_4–Mn_2^{2+}–$NADPH_4$ Complex[a]

displacer	displacer concn (mM)	A_1	A_2	k_1 (s^{-1})	k_2 (s^{-1})
$NADP^+$	1.0	406 ± 65	387 ± 20	846 ± 170	97 ± 5
$NADP^+$	0.83	381 ± 77	357 ± 46	804 ± 331	96 ± 9
$NADP^+$	3.2	345 ± 80	339 ± 16	684 ± 292	89 ± 11
ATPR	1.0	406 ± 52	220 ± 28	645 ± 150	99 ± 17

[a] The reaction mixtures contain malic enzyme subunits (7.4–10 μM) and NADPH at a NADPH/E ratio of 0.95–1.2; $MnCl_2$, 0.2 mM.

dissociation reaction. A more satisfactory fitting is obtained to the sum of two exponentials according to eq 1 as shown in Figure 2C. The parameters thus obtained for four experiments are summarized in Table II. The rate constant of the slower reaction with a mean value of 96.0 s^{-1} (k_2, Table II) corresponds to, but is a better estimate than, the value (135 s^{-1}) obtained for a single exponential function. The rate constant (645–846 s^{-1}) and amplitude of the fast phase (k_1 and A_1, respectively, in Table II) are highly variable, since 75–90% of this reaction occurs in the dead time (2 ms) of the instrument and the remainder is largely obscured by the slower reaction.

As the amplitudes of the two reactions are not obviously different, and there are only two Mn^{2+}-liganded subunits on the ternary E_4–Mn_2^{2+}–$NADPH_4$ tetramer complex, the fast reaction is assigned to NADPH dissociation from the Mn^{2+}-deficient subunits, and the slower reaction with a rate constant of 96.0 s^{-1} is assigned to NADPH dissociation from the two Mn^{2+}-liganded subunits.

Effect of Malate on the Kinetics of NADPH Dissociation. In recent studies employing the equilibrium dialysis technique (Pry & Hsu, 1980), it was shown that malate binds to malic enzyme in the presence of Mn^{2+} and NADPH and that tightly bound Mn^{2+} promotes the binding of malate to two substrate sites with a k_t of 22–23 μM and two additional sites with a k_w of 350–400 μM per enzyme tetramer. Experiments are therefore carried out in the presence of 0.2 mM $MnCl_2$ and variable amounts (0.075–7.0 mM) of malate to saturate only tight or tight and weak substrate sites. In all cases, ATPR is used as the displacement reagent to avoid catalytic turnover. In these experiments, biphasic progress curves are obtained with no observable fast reaction attributable to NADPH dissociation from E–NADPH but with an additional very slow reaction due to the presence of malate. The progress curves are fitted to the sum of two exponentials, except those obtained at the highest malate levels (2.5–7.0 mM) which are fitted to a single first-order process. The parameters are summarized in Table III. Rate constants for the two dissociation reactions are independent of malate concentration, yielding mean values of 100 s^{-1} (six experiments) and 2.69 s^{-1} (eight experiments). The amplitude of the very slow reaction increases relative to the reaction occurring at a rate of 100 s^{-1} with increasing malate concentration, as shown by comparison of typical experiments at 0.3 (Figure 3A) and 1.0 mM malate (Figure 3B) where more than 90% of the observed fluorescence decrease is accounted for by the very slow reaction at the 2.69-s^{-1} rate.

Since malate occupies two tight substrate sites at lower concentrations (≤0.1 mM), and both tight and weak sites at the high concentration (7.0 mM) employed, the rate constants of 100 and 2.69 s^{-1} are therefore assigned, respectively, to NADPH dissociation from E_4–Mn_2^{2+}–$NADPH_4$–dimalate and E_4–Mn_2^{2+}–$NADPH_4$–tetramalate complexes. A rough approximation of the percentage of tetramalate in a mixture

Table III: Parameters of NADPH Dissociation from E_4–Mn_2^{2+}–$NADPH_4$–Dimalate and E_4–Mn_2^{2+}–$NADPH_4$–Tetramalate Complexes[a]

$[Mn^{2+}]$ (mM)	[malate] (mM)	k_1 (s^{-1})	k_2 (s^{-1})	% tetramalate complex[b]
0.2	0.075[c]	94.6 ± 7.1	2.82 ± 0.08	1
	0.1[c]	93.0 ± 2.1	2.20 ± 0.04	1
	0.2[c]	121 ± 20	2.71 ± 0.02	23
	0.3[c]	96.5 ± 6.4	2.69 ± 0.02	21
	0.6[c]	95.2 ± 19.3	2.71 ± 0.02	34
	1.0[c]	97.6 ± 25	2.74 ± 0.02	48
	2.5[d]		2.83 ± 0.02	72
	7.0[d]		2.82 ± 0.01	82
5.0	1.0[d]		3.03 ± 0.01	
10.0	7.0[d]		3.21 ± 0.01	

[a] The reaction mixtures contain malic enzyme subunits (5–10 μM) and NADPH equal to or twice the enzyme concentration, $MnCl_2$, and malate at the indicated levels. ATPR (1.0 mM) is used as the displacement reagent. The rate constants are the means (±SD) of values estimated by nonlinear regression fitting of two to five progress curves in each experiment. Values for experiments using 0.3 mM malate are averages of three experiments. [b] The percentage of tetramalate complex is the fraction of E_4–Mn_2^{2+}–$NADPH_4$–tetramalate in a mixture containing this complex and the complex E_4–Mn_2^{2+}–$NADPH_4$–dimalate and equals $(A_2/5.84)/[A_1 + (A_2/5.84)]$. The amplitude of the slow phase (A_2) is obtained by nonlinear regression analysis of the fluorescence decay curve extrapolated to zero time and is divided by 5.84 to compensate for the greater fluorescence enhancement of the tetramalate complex. The amplitude of the faster phase (A_1) is the difference between the total fluorescence change and A_2, with the former estimated by subtracting the fluorescence at the end of the reaction recorded at 20 s minus the ATPR fluorescence from the fluorescence of a reaction blank containing all reagents except ATPR. [c] Fitted to two exponentials. [d] Fitted to a single exponential.

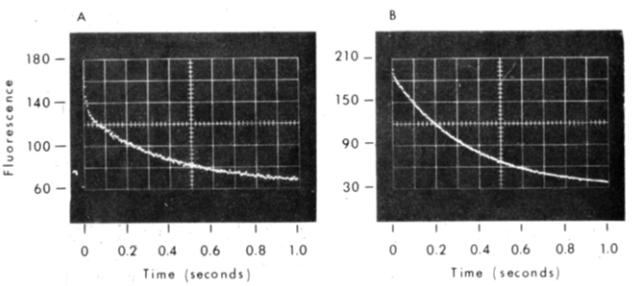

FIGURE 3: Time courses of NADPH dissociation from the enzyme complex in the presence of Mn^{2+} and malate. The final concentrations are the following: enzyme subunits, 10.0 μM; NADPH, 10.0 μM; $MnCl_2$, 0.2 mM; malate, 0.3 (A) and 1.0 mM (B). Displacement reagent, 1.0 mM ATPR.

containing both complexes may be calculated from the relative amplitudes of the two reactions corrected for differences in fluorescence enhancement, as shown in Table III.

At high concentrations, Mn^{2+} also binds to two to four weak metal sites. In experiments employing the quaternary tetramalate complex, increasing the Mn^{2+} concentration from 0.2 to 5.0–10.0 mM is accompanied by a small increase in the rate constant of NADPH dissociation (≃10%, Table III), as might be expected from an ionic strength effect. The true rate constant for the complex containing weakly bound Mn^{2+} cannot be determined, since as shown in the fluorescence titration curve of Figure 4 the Mn^{2+} ligand completely abolishes the fluorescence enhancement of the reduced nucleotide.

Initial Rate Measurements. The maximum turnover number in the absence of malate inhibition is estimated by initial rate measurements at saturating $NADP^+$ concentration (220

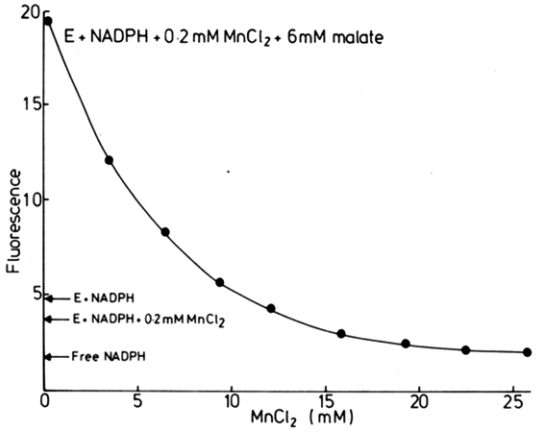

FIGURE 4: Fluorescence titration of the E_4–Mn_2^{2+}–$NADPH_4$–tetramalate complex with $MnCl_2$. The reaction mixture initially contains enzyme subunits (1.98 μM), NADPH (0.74 μM), malate (6 mM), and $MnCl_2$ (0.2 mM) in triethanolamine hydrochloride buffer, pH 7.0. The titration is carried out with 0.1 M $MnCl_2$, and the fluorescence is measured at excitation and emission wavelengths of 340 and 460 nm and is corrected for dilution. The fluorescence levels of E_4–$NADPH_4$, E_4–Mn_2^{2+}–$NADPH_4$, and free NADPH are shown for comparison.

Table IV: Steady-State Kinetic Constants for the Oxidative Decarboxylation of Malate[a]

kinetic constant	expt 1	expt 2
ϕ_0 (s)	0.0196 ± 0.00027	0.0180 ± 0.00029
ϕ_1 (μM s)	0.916 ± 0.009	0.964 ± 0.009
ϕ_2 (μM s)	0.0841 ± 0.008	0.148 ± 0.007
ϕ_{12} (μM^2 s)	10.2 ± 0.29	9.78 ± 0.25
K_m(malate) (μM)	46.8 ± 0.80	53.5 ± 0.99
K_m(Mn^{2+}) (μM)	4.29 ± 0.42	8.19 ± 0.40
$V_0/[E]$ (s^{-1})	51.0 ± 0.71	55.5 ± 0.88

[a] The experiments are carried out as described in the Figure 5 legend.

μM) and variable malate and Mn^{2+} concentrations in 50 mM triethanolamine hydrochloride buffer, pH 7.0, at 30 °C. The resulting data are analyzed with a computer program devised by N. V. McFerran (unpublished) to evaluate the constants in the equation

$$\frac{[E]}{V_0} = \phi_0 + \frac{\phi_1}{[\text{malate}]} + \frac{\phi_2}{[Mn^{2+}]} + \frac{\phi_{12}}{[\text{malate}][Mn^{2+}]}$$

using $(V_0/[E])^2$ as weights in the primary plots. [E] is the enzyme subunit concentration. The parameters obtained from two experiments are shown in Table IV. The mean value for the maximum turnover number per enzyme subunit ($V_0/[E]$) is 53.3 ± 3.0 s^{-1}.

Initial rates are also determined by optical density measurements at 340 nm in the stopped-flow apparatus using 0.2 mM $MnCl_2$ and a wide range of malate concentrations from 40 μM to 5.0 mM. In these experiments, enzyme and malate are placed in separate syringes in order to observe the time course of substrate inhibition upon combination. Typical progress curves are shown in Figure 5. At 100 μM malate, the time course is linear (Figure 5A), whereas at 2.5 mM malate the rate decreases during the first $\simeq$0.5 s to a steady-state inhibited value. This relatively slow development of substrate inhibition confirms our previous observation (Reynolds et al., 1978). Evidence in support of such behavior is further obtained from a double-reciprocal plot (Figure 6). At inhibiting levels (>500 μM) of malate, the rates during the first 50 ms obey Michaelian kinetics and are therefore true initial rates of the uninhibited enzyme.

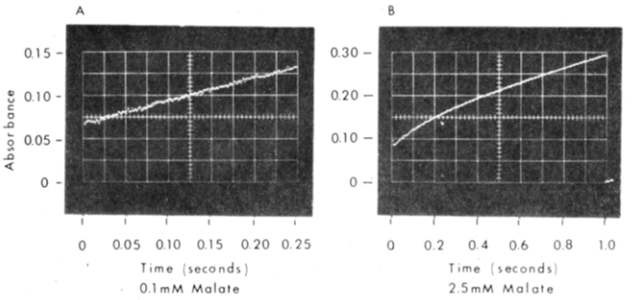

FIGURE 5: Initial rate measurements in the stopped-flow apparatus. The reaction mixtures contain enzyme subunits (0.57 μM), $NADP^+$ (0.5 mM), $MnCl_2$ (0.2 mM), and malate [100 μM (A) and 2.5 mM (B)] in triethanolamine hydrochloride buffer, pH 7.0. Temperature, 30 °C. Syringe 1 contains enzyme, $MnCl_2$, and $NADP^+$; syringe 2 contains $MnCl_2$ and malate.

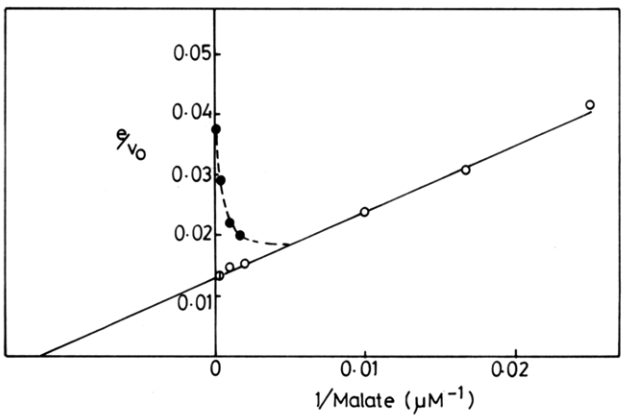

FIGURE 6: Double-reciprocal plot of initial and inhibited rates in the stopped-flow apparatus. The reaction mixtures are as shown in the Figure 5 legend except malate concentrations are varied as indicated. (●) Initial rates; (○) inhibited rates. At malate concentrations where inhibition occurs, the initial rates are obtained from the first 50 ms of the reaction, and the inhibited rates are obtained after constant steady-state turnover is reached (>0.5 s).

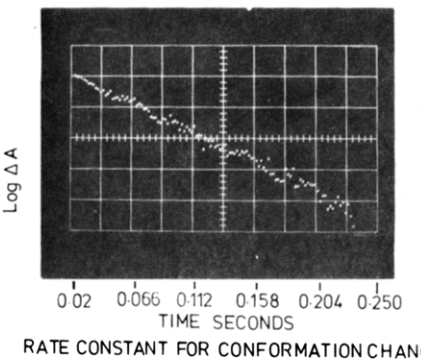

FIGURE 7: Semilogarithmic plot of ΔOD vs. time. The experiment is carried out as described in the Figure 6 legend except with 60 μM $MnCl_2$ and 5.0 mM malate. ΔOD is the difference between the observed absorption and the absorption obtained from extrapolation of the inhibited steady-state rate to zero time. The slope of this plot has been shown by Dalziel et al. (1978) to equal $-k/2.3$.

Table V: First-Order Rate Constants for the Transition of Initial to Inhibited Rates

	k (s^{-1})	
[malate] (mM)	60 μM [Mn^{2+}]	200 μM [Mn^{2+}]
0.6	5.0	5.2
1.0	5.3	5.3
2.5	6.1	6.1
5.0	6.9	7.1

The transition from the initial to the inhibited rate at high malate concentration follows a first-order process, as indicated by the linear log ΔOD vs. time plot of a typcial experiment shown in Figure 7. The rate constants from a number of experiments are shown in Table V. In the range of concentrations tested, this parameter is unaffected by Mn^{2+} and increased by 40% with an 8-fold increase of malate to a limiting value of 7.0 ± 0.1 s^{-1} at 5.0 mM malate.

Discussion

In previous reports (Pry & Hsu, 1980; Hsu & Pry, 1980; Hsu, 1982, 1983), we have delineated details of a half-of-the-sites model for the oxidative decarboxylation reaction catalyzed by malic enzyme. The proposed model is based on cumulative evidence for negative cooperativity between subunits obtained by transient and steady-state kinetic studies, by equilibrium binding experiments with malate, the transition-state analogue oxalate, and the metal activator Mn^{2+}, and by chemical modification with the affinity label bromopyruvate (Reynolds et al., 1978; Vernon & Hsu, 1983; Hsu, 1983). Stopped-flow data showing half-size burst of enzyme-bound NADPH (Reynolds et al., 1978) are in support of this model. Evidence for NADPH release as the rate-limiting step (Schimerlik et al., 1977; Reynolds et al., 1978) is also taken into account.

Malic enzyme is depicted to exist as a homotetramer in the free state, with each subunit containing a "complete" active site capable of binding all reactants. During the catalytic reaction, binding of Mn^{2+} induced strong site–site cooperative interactions, and this activator and malate each bind anticooperatively to two types of functionally distinct high-affinity (tight) and low-affinity (weak) sites of two each. The enzyme is maximally active with $NADP^+$ occupying four equivalent nucleotide sites, malate occupying two tight substrate sites, and Mn^{2+} occupying tight or both tight and weak metal sites. Following the sequential release of CO_2 and pyruvate, dissociation of the final product NADPH limits the rate of reaction. Binding of malate on weak (regulatory) sites in the absence of weakly bound Mn^{2+} causes substrate inhibition by inhibiting NADPH dissociation at the adjoining tight sites undergoing catalysis, whereas binding of Mn^{2+} as well on the weak sites prevents this inhibition. Since only half of the enzyme sites are simultaneously active in the catalytic process, it follows that NADPH should dissociate at a rate twice the maximum turnover rate per enzyme site and that this rate is reduced under conditions of malate inhibition.

In the present work, the kinetics of NADPH dissociation from the abortive E_4–$NADPH_4$, E_4–Mn_2^{2+}–$NADPH_4$, E_4–Mn_2^{2+}–$NADPH_4$–dimalate, and E_4–Mn_2^{2+}–$NADPH_4$–tetramalate complexes are examined in the stopped-flow apparatus. NADPH has been shown to bind four independent, equivalent sites on the unliganded enzyme with a K_D of 1.1 μM at pH 7.0, 30 °C (Pry & Hsu, 1980). The occurrence of a single first-order rate process associated with NADPH dissociation from the binary complex confirms this "all-of-the-sites" behavior. From the above K_D value and a dissociation rate constant of 427 s^{-1} (Table I, see reference to Table I under Results) a second-order association constant of 3.8 × 10^8 M^{-1} s^{-1} is calculated which is close to the limit for diffusion-controlled processes (Gutfreund, 1972).

While the time course for the dissociation of NADPH from the ternary E_4–Mn_2^{2+}–$NADPH_4$ complex may be fitted by the theoretical curve generated for a single first-order process with a rate constant of 135 s^{-1}, more satisfactory fitting is obtained for two simultaneous first-order processes (Figure 2C vs. Figure 2B). The rate constant for the slower process—dissociation of NADPH from the Mn^{2+}-liganded subunit (k_2 = 96 s^{-1}, Table II)—is estimated with good precision. The faster reaction cannot be accurately quantitated but is expected to be the release of NADPH from the Mn^{2+}-deficient E–NADPH subunit complex analogous to that from the E_4–$NADPH_4$ complex.

Bisphasic kinetic behavior is also observed for the dissociation of NADPH from complexes prepared in the presence of malate, yielding rate constants of 100 and 2.69 s^{-1} correpsonding to those for the E_4–Mn_2^{2+}–$NADPH_4$–dimalate and E_4–Mn_2^{2+}–$NADPH_4$–tetramalate complexes, respectively. The former is identical with the value of 96 s^{-1} within experimental error. Since in the E_4–Mn_2^{2+}–$NADPH_4$–dimalate complex the tightly bound malate is expected to occupy the subunit site containing Mn^{2+} ligand, it follows that dissociation of NADPH from this site is unaffected by malate occupancy. The absence of a fast reaction (k = 427 s^{-1}) further indicates that tightly bound malate decreases NADPH dissociation from the adjacent Mn^{2+}- and malate-deficient subunits. Moreover, dissociation of NADPH from both Mn^{2+}-liganded and Mn^{2+}-deficient subunits in the E_4–Mn_2^{2+}–$NADPH_4$–tetramalate complex is reduced ≃37-fold by the weakly bound malate (Table III).

The ligand-induced changes of the kinetic behavior of NADPH dissociation from its complexes with malic enzyme (k = 427, 96–100, and 2.69 s^{-1}) strongly imply both intra- and intersubunit cooperative interactions with resultant alteractions in the local environment of the nucleotide binding site. The biphasic kinetic pattern seen at intermediate malate levels where dimalate and tetramalate complexes coexist suggests similar biphasic equilibrium binding behavior and the likelihood that the K_D's of the reduced nucleotide determined at comparable concentrations of malate (Pry & Hsu, 1980) represent only average values because of the low resolving power of Scatchard analysis.

Since high Mn^{2+} concentration relieves malate inhibition (Hsu et al., 1976; Reynolds et al., 1978; Hsu & Pry, 1980), a parallel increase in the rate of NADPH dissociation is expected. However, a determination of the dissociation rate constant of reduced nucleotide from the quaternary E_4–Mn_{4-6}^{2+}–$NADPH_4$–tetramalate complex containing weakly bound Mn^{2+} is precluded by the lack of fluorescence enhancement (Figure 4). This may be due to metal ion induced quenching of fluorescence, or complete dissociation of bound nucleotide which will result in the relief of substrate inhibtion in catalysis. Further experiments are required to clarify this point.

In steady-state analysis, kinetic constants obtained by the fluorometric method (Table IV) are in good agreement with those obtained spectrophotometrically in earlier work (Hsu & Pry, 1980). In the half-of-the-sites model, NADPH dissociates from the Mn^{2+}-containing subunit (i.e., E–Mn^{2+}–NADPH) of the transient product complex E_4–Mn_2^{2+}–$NADPH_2$–$NADP_2$. A comparison of the maximum turnover rate (V_0/[E]) of 53.3 ± 3.0 s^{-1} calculated on a subunit basis with a NADPH dissociation rate constant of 96 s^{-1} from the E–Mn^{2+}–NADPH subunit of the E_4–Mn_2^{2+}–$NADPH_4$ complex (see Results) shows that within experimental error the latter doubles the rate of turnover. Notwithstanding the difference in the "redox" state of the nucleotide ($NADP^+$) on the noncatalytic subunit of the transient product complex and the abortive complex (NADPH), this 2:1 ratio provides strong support for the proposed model.

At infinite malate concentration, steady-state turnover of the enzyme with tightly bound Mn^{2+} is inhibited 93% (Hsu

& Pry, 1980). The parallel decrease (from 96 to 2.69 s^{-1}, 97%) in the NADPH dissociation rate (Table III) provides unequivocal evidence for NADPH release as the rate-limiting step in oxidative decarboxylation, and that inhibition of this step is responsible for substrate inhibition. In a previous study (Reynolds et al., 1978), the slow onset of substrate inhibition was attributed to a slow conformational change of the quaternary malate complex from an active to a less active (7%) form. The first-order time course observed for the transition process (Figure 7) is consistent with such a mechanism which can be written as

$$E_4\text{–}Mn_2^{2+}\text{–}NADPH_2\ (NADP^+)_2\text{–tetramalate} \xrightarrow[t_{1/2} = 0.1\ s]{k = 7\ s^{-1}} E_4'\text{–}Mn_2^{2+}\text{–}NADPH_2\ (NADP^+)_2\text{–tetramalate}$$

in terms of enzyme–ligand complexes defined by the postulated model (Hsu & Pry, 1980). E and E′ are active and partially active enzyme complexes, respectively. Conversely, our results are at variance with the alternative possibility of slow addition of malate in the second-order association reaction which requires a linear dependence of the first-order rate constant for transition (k) on the ligand concentration.

Registry No. NADPH, 53-57-6; Mn, 7439-96-5; L-malic acid, 97-67-6; malic enzyme, 9028-47-1.

References

Chang, G. G., & Hsu, R. Y. (1973) *Biochem. Biophys. Res. Commun. 55*, 580–587.

Chang, G. G., & Hsu, R. Y. (1977) *Biochemistry 16*, 311–320.

Dalziel, K. (1961) *Biochem. J. 80*, 440–445.

Dalziel, K. (1962) *Biochem. J. 84*, 244–254.

Dalziel, K., McFerran, N., Matthews, B., & Reynolds, C. H. (1978) *Biochem. J. 171*, 743–750.

Engle, P. C., & Dalziel, K. (1968) *Biochem. J. 105*, 691–695.

Fatania, H. R., Matthews, B., & Dalziel, K. (1982) *Proc. R. Soc. London, Ser. B 214*, 369–387.

Gibson, O. H., & Milnes, L. (1964) *Biochem. J. 91*, 161–171.

Gutfreund, H. (1972) *Enzymes: Physical Principles*, p 159, Wiley, New York.

Hsu, R. Y. (1982) *Mol. Cell. Biochem. 43*, 3–26.

Hsu, R. Y. (1983) *Steenbock-Lilly Symposium on the Biochemistry of Metabolic Processes* (Lennon, D. F., Stratman, F. W., & Zahlten, R. N., Eds.) pp 259–272, Elsevier Scientific Publishing Co., New York.

Hsu, R. Y., & Lardy, H. A. (1967a) *J. Biol. Chem. 242*, 520–526.

Hsu, R. Y., & Lardy, H. A. (1967b) *J. Biol. Chem. 242*, 527–532.

Hsu, R. Y., & Pry, T. A. (1980) *Biochemistry 19*, 962–968.

Hsu, R. Y., Lardy, H. A., & Cleland, W. W. (1967) *J. Biol. Chem. 242*, 5315–5322.

Hsu, R. Y., Mildvan, A. S., Chang, G. G., & Fung, C. H. (1976) *J. Biol. Chem. 251*, 6574–6583.

Nevaldine, B. H., Bassel, A. R., & Hsu, R. Y. (1974) *Biochim. Biophys. Acta 336*, 283–293.

Pry, T. A., & Hsu, R. Y. (1978) *Biochemistry 17*, 4024–4029.

Pry, T. A., & Hsu, R. Y. (1980) *Biochemistry 19*, 951–962.

Reynolds, C. H., Hsu, R. Y., Matthews, B., Pry, T. A., & Dalziel, K. (1978) *Arch. Biochem. Biophys. 189*, 309–316.

Schimerlik, M. I., Grimshaw, C. E., & Cleland, W. W. (1977) *Biochemistry 16*, 571–576.

Vernon, C. M., & Hsu, R. Y. (1983) *Arch. Biochem. Biophys. 225*, 296–305.

Purification and Properties of Two Hemagglutinins of the Mushroom *Laccaria amethystina*†

Jean Guillot,* Liliane Genaud, Josée Gueugnot, and Mireille Damez

ABSTRACT: Two lectins of different specificity were isolated from the mushroom *Laccaria amethystina* by affinity chromatography with stromas of group O human erythrocytes included in polyacrylamide gel. The more abundant lectin (LAL) was eluted by lactose, which specifically inhibited the agglutination of phenotype A and O erythrocytes and the protozoan *Crithidia fasciculata*. Its molecular weight determined by sodium dodecyl sulfate gel electrophoresis was 17 500, and its structure is apparently monomeric. It appeared homogeneous by electrophoresis but showed microheterogeneity by isoelectric focusing. The other lectin (LAF) was eluted by L-fucose. It possesses anti-H properties, since its agglutinating activity was greater toward phenotype O and A_2 erythrocytes than toward A_1 erythrocytes. Agglutination of erythrocytes and various protozoa was specifically inhibited by L-fucose. Its molecular weight was 16 000, and its structure is apparently monomeric. Its homogeneity was confirmed by polyacrylamide gel electrophoresis and isoelectric focusing.

The occurrence in mushrooms of substances active toward red blood cells of human or animal origin has been recognized since the beginning of the century [for a general review, see Coulet et al. (1970b)]. There are early reports (Ford, 1911; Friedberger & Brossa, 1912; Galli-Valerio & Bornand, 1916) of attempts to relate the toxicity of some species to their hemolytic or hemagglutinant potency. Hemagglutinins occur extensively in mycetes, including edible species; their rate of occurrence in mycetes exceeds that found in higher plants. Systematic explorations covering more than 600 species (Coulet & Merland, 1960a,b; Coulet et al., 1964, 1970a; Merland & Coulet, 1961) have revealed the presence of lectins in about 30% of the higher fungi studied. In addition, specificity with regard to human red blood cells has been found in 18% of the active species: anti A + B (Elo et al., 1951; Guillot & Coulet, 1974), anti B (Coulet & Marche, 1962; Mäkelä et al., 1959), anti B + H (Elo & Estola, 1952), and anti H (Kogure, 1973).

The presence of lectins in mushrooms of the genus *Laccaria* was first demonstrated in *Laccaria amethystina* by Elo &

† From the Department of Botany and Microbiology, Faculty of Pharmaceutical Sciences, University of Clermont I, 63001 Clermont-Ferrand, France. *Received January 18, 1983.*

0006-2960/83/0422-5365$01.50/0 © 1983 American Chemical Society